

1

2 **Title:** Topological basis of epileptogenesis in a model of severe cortical trauma

3 **Authors:** Vladislav Volman^{1,2}, Terrence J. Sejnowski^{1,2,3}, Maxim Bazhenov⁴

4

5 1. Howard Hughes Medical Institute, Computational Neurobiology Laboratory, The Salk
6 Institute for Biological Studies, La Jolla, CA 92037, USA

7 2. Center for Theoretical Biological Physics, University of California San Diego, La Jolla,
8 CA 92093, USA

9 3. Division of Biological Sciences, University of California, San Diego, La Jolla, CA
10 92093, USA

11 4. Department of Cell Biology and Neuroscience, University of California, Riverside,
12 Riverside, CA 92521, USA

13

14 **Running title:** Epileptogenesis in severely traumatized cortex

15

16 **Corresponding author:**

17 Dr. Maxim Bazhenov

18 Department of Cell Biology and Neuroscience, University of California, Riverside,
19 Riverside, CA 92521, USA.

20 Email: Maksim.Bazhenov@ucr.edu

21

22

23

24

25

26

27 **Abstract**

28

29 Epileptic activity often arises after a latent period following traumatic brain injury. Several
30 factors contribute to the emergence of post-traumatic epilepsy, including disturbances to ionic
31 homeostasis, pathological action of intrinsic and synaptic homeostatic plasticity and remodeling
32 of anatomical network synaptic connectivity. We simulated a large-scale biophysically realistic
33 computational model of cortical tissue to study the mechanisms underlying the genesis of post-
34 traumatic paroxysmal epileptic-like activity in the deafferentation model of a severely
35 traumatized cortical network. Post-traumatic generation of paroxysmal events did not require
36 changes of the structural connectivity. Rather, network bursts were induced following the action
37 of homeostatic synaptic plasticity which selectively influenced functionally dominant groups of
38 intact neurons with preserved inputs. This effect critically depended on the spatial density of
39 intact neurons. Thus, in the deafferentation model of post-traumatic epilepsy, trauma-induced
40 change in functional (rather than anatomical) connectivity might be sufficient for
41 epileptogenesis.

42

43 **Keywords:** homeostatic plasticity, paroxysmal discharge, seizure.

44

45

46

47

48

49

50

51

52 **Introduction**

53

54 Interictal epileptiform discharges (IEDs), characterized by brief repetitive (~200-500 ms) bursts
55 of highly correlated population activity, are often considered as an important diagnostic feature
56 of epileptic seizures (Dzhala and Staley 2003; Wendling et al. 2005). Despite the fundamental
57 significance of IEDs, the mechanisms responsible for their generation in epileptic brains are still
58 elusive (de Curtis and Avanzini 2001; Keller et al. 2010). IEDs could reflect complex network
59 interactions in heterogeneous neuronal populations (Keller et al. 2010), which depend on many
60 different network organization parameters such as connectivity and topological correlations
61 (Srinivas et al. 2007; Bogaard et al. 2009).

62

63 To address this question, we designed a large-scale model of a cortical network to study the
64 characteristics of post-traumatic IED activity, which often arises *in vivo* after a latent period that
65 follows traumatic brain injury (TBI) (Pitkanen et al. 2006). Understanding how brain trauma
66 affects the propensity to observe IEDs can help reveal the ways in which a traumatized brain
67 can become epileptic. Earlier studies indicated that in the traumatized network, adjustable
68 remodeling of network's anatomical connectivity can result in transition from normal
69 (asynchronous) to burst-like collective activity (Dyhrfeld-Johnsen et al. 2007; Morgan and
70 Soltesz 2008). Other studies suggested that intrinsic and synaptic homeostatic plasticity
71 (Turrigiano et al. 1998) after brain trauma may contribute to epileptogenesis (Houweling et al.
72 2005; Avramescu and Timofeev 2008; Frohlich et al. 2008; Timofeev et al. 2010).

73

74 In this study, we show that the transition to IED does not necessarily rely on changes in the
75 network topology. Rather, the emergence of paroxysmal bursts critically depends on the
76 functional connectivity that is primarily determined by the spatial distribution of trauma-

77 surviving (intact) neurons and the dominant synaptic connections between them. We further
78 show that topological determinants of this intact subnetwork only weakly affect the rate of post-
79 traumatic interictal activity; rather, the spatial density of intact neurons is the pivotal parameter.
80 This suggests a new, previously overlooked role for the spatial pattern of brain trauma in
81 determining the chances of developing pathological activity.

82

83

84

85 **Materials and Methods**

86

87 *The cortical network model*

88 A cortical network was modeled as a 2D network (80 x 80 neurons) in which each neuron could
89 establish synapses with its peers with probability $p_C = 0.6$ within its local footprint (10 x 10
90 neurons). Pyramidal neurons constituted 80% of network population (5120 out of 6400
91 neurons), and inhibitory neurons constituted the remaining 20% (1280 out of 6400 neurons).
92 We have not implemented layer specific features in the model because our goal was to define
93 general properties of a cortical network responding to traumatic intervention. This is a common
94 approach that has both its advantages (many layer specific properties are not well known and
95 generic model captures common dynamics of the cortical network) and disadvantages (layer
96 specific features, e.g., predisposition of the specific layers or areas to the epileptogenesis cannot
97 be tested).

98

99 Parameters were tuned such that in the baseline conditions, model pyramidal (PY) and
100 inhibitory (IN) neurons fired with average rates of 5 and 10 Hz, respectively (Figure 2A). For
101 each model neuron, the current equation was

$$102 \quad C_m \frac{dV_m}{dt} = -I_{ion}(t) + I_{syn}(t) + I_{EX}(t) \quad (1)$$

103 The ionic current evolved according to (Prescott et al. 2006):

$$104 \quad I_{ion}(t) = G_{Na} w(V_m)(V_m - 50) + G_K m_\infty(V_m)(V_m + 100) + G_L(V_m + 70) + G_A(t)(V_m + 100) \quad (2)$$

105 The fraction of open Na channels was

$$106 \quad \frac{dw}{dt} = 0.15(w_\infty(V_m) - w(V_m)) \cosh((V_m + 2)/42) \quad (3)$$

107 The steady-state fractions of Na and K channels were, correspondingly

108 $w_{\infty}(V_m) = 0.5(1 + \tanh((V_m + 2)/21))$; $m_{\infty}(V_m) = 0.5(1 + \tanh((V_m + 1.2)/23))$ (4)

109 Adaptation conductance, $G_A(t)$, was nonzero only for PY neurons

110 $G_A(t) = (3 \text{ mS/cm}^2)z(t)$ (5)

111 $\frac{dz}{dt} = 0.005 \cdot \left(-z + \frac{1}{1 + \exp(-V_m/5)} \right)$ (6)

112 Values of other parameters:

113 $G_{Na} = 10 \text{ mS/cm}^2$, $G_K = 10 \text{ mS/cm}^2$, $G_L = 1.3 \text{ mS/cm}^2$, $C_m = 1 \mu\text{F/cm}^2$.

114

115 *Synaptic dynamics*

116 Synaptic transmission was modeled as a deterministic process in which both AMPA and

117 GABAa conductances were described as

118 $\frac{dg_X}{dt} = -\frac{g_X}{\tau_D} + G_X D \delta(t - t_{SPIKE})$ (7)

119 where $\tau_D = 5 \text{ ms}$ was the time of synaptic conductance decay. Per spike synaptic conductances

120 were: $G_{PP} = 74.4 \mu\text{S/cm}^2$, $G_{IP} = 89.28 \mu\text{S/cm}^2$, $G_{PI} = 372 \mu\text{S/cm}^2$, $G_{II} = 74.4 \mu\text{S/cm}^2$.

121 NMDA conductance dynamics was modeled as

122 $g_{NMDA}(t) = \frac{g_S(t) - g_F(t)}{1 + 0.264 \exp(-0.06V_m)}$ (8)

123 with

124 $\frac{dg_{F,S}}{dt} = -\frac{g_{F,S}}{\tau_{F,S}} + G_{NMDA} D \delta(t - t_{SPIKE})$ (9)

125 NMDA receptor activation parameters were: $G_{NMDA} = 8.928 \mu\text{S/cm}^2$, $\tau_F = 2 \text{ ms}$, $\tau_S = 80 \text{ ms}$.

126 The parameter D accounted for short-term synaptic depression at AMPA/NMDA synapses:

127 $\frac{dD}{dt} = \frac{1-D}{\tau_R} - U \delta(t - t_{SPIKE})$ (10)

128 Depression parameters were: $\tau_R = 0.8 s$, $U = 0.07$. All synaptic currents were related to their
129 conductances by $I_X(t) = -g_X(t)(V_m - E_X)$, with $E_{AMPA} = E_{NMDA} = 0 mV$, $E_{GABA} = -70 mV$. In
130 addition to network current, each model neuron received an excitatory current
131 $I_{EX}(t) = -g_{EX}(t)(V_m - E_{EX})$ from “the rest” of the cortex. Synaptic conductance of this current
132 evolved according to $\frac{dg_{EX}}{dt} = -\frac{g_{EX}}{\tau_{EX}} + G_{EX}\delta(t - t_{EX})$, and was stimulated at times t_{EX} at the
133 baseline Poisson rate of $\nu_{EX} = 100 Hz$. Other parameters of external stimulation were
134 $G_{EX} = 300 \mu S/cm^2$; $\tau_{EX} = 5 ms$; $E_{EX} = 0 mV$. This external stimulation will be henceforth
135 referred to as “afferent excitation”. This afferent excitation was responsible for the generation of
136 background electrical activity in network models. Afferent excitation was present throughout
137 the simulations in all model neurons, albeit its intensity for a given neuron depended on the
138 specific trauma scenario that we studied, as described below.

139

140 *Trauma*

141 In its simplest form, trauma can be described as deafferentation, following which the amount of
142 external input to the network is reduced (Grafstein and Sastry 1957; Prince and Tseng 1993). In
143 the present model, we assumed that deafferentation is parameterized by both the number of
144 deafferented neurons and the reduction in the rate of their afferent excitation. Thus, the trauma
145 in our model was described by two parameters: f_D , fraction of deafferented neurons, and r_D ,
146 the remaining (relative to baseline scenario of $\nu_{EX} = 100 Hz$) rate of afferent excitation. As an
147 example, $(f_D = 0.3, r_D = 0.4)$ describes a scenario in which the external stimulation rate to 30
148 percent of randomly picked neurons is reduced to 40 percent (40 Hz) of its value in “healthy”
149 network (100 Hz). We mainly considered scenarios with almost complete deafferentation. A
150 small number of model neurons (1 to 5 percent of total network population, labeled as N_I)

151 preserved their external afferent inputs after the trauma (that is, at all times after the trauma the
152 rate of afferent excitation to these neurons was the same as in the baseline model,
153 $\nu_{EX} = 100 Hz$). These neurons were referred to as “intact” neurons and were distributed in
154 space as described below.

155

156 *Spatial density of intact model neurons*

157 One of our main results is the observation that the rate of paroxysmal discharges in severely
158 traumatized network critically depends on the distribution of intact neurons – the neurons that
159 preserve intact afferent input after deafferentation. To vary the spatial distribution of these intact
160 neurons, we defined their spatial density, as follows. We first defined the area in which intact
161 neurons could be distributed as a square (symmetric with respect to the center of our 2D lattice
162 on which the network was built) of side L_I (in lattice units). A predefined number N_I of
163 neurons were then randomly selected from all $L_I \times L_I$ neurons in the region of interest (each
164 lattice site in our 2D lattice could accommodate only one model neuron). These selected
165 neurons preserved their input after deafferentation. All other neurons in the network were
166 deafferented. The ratio, $\rho_I = N_I / (L_I \times L_I)$, then defined the spatial density of intact neurons
167 within $L_I \times L_I$ area after deafferentation. According to this definition, $\rho_I = 1$ implies that all the
168 neurons within selected $L_I \times L_I$ area were intact and all the deafferented neurons were
169 distributed outside this area. $\rho_I = 0$ implies that all the neurons of the network were
170 deafferented. Note that this definition of “intact neuron density” applies only to the case of
171 traumatized network, when the population of model neurons can be subdivided into
172 “deafferented” and “intact” on the basis of the afferent excitation they receive.

173

174 *Homeostatic synaptic plasticity*

175 Following earlier studies (Houweling et al. 2005; Frohlich et al. 2008), we employed an
 176 approximation whereby homeostatic adjustments of collateral synaptic conductances (of intra-
 177 network connections) were calculated at the end of every 4 seconds of simulation on the basis of
 178 activity during the preceding 4 seconds. The following equations were applied to adjust
 179 collateral synaptic conductances

$$180 \quad G_{PP} = G_{PP} + 10^{-3}(\nu_0 - \bar{\nu})G_{PP} \quad ; \quad G_{PI} = G_{PI} - 5 \cdot 10^{-4}(\nu_0 - \bar{\nu})G_{PI} \quad (11)$$

181 in which $\bar{\nu}$ is the averaged (over all PY neurons in the network) firing rate during the preceding
 182 4 seconds, and ν_0 is the target firing rate (5 Hz). Longer monitoring intervals (8 and 12
 183 seconds) affected the rate with which the network approached its post-traumatic steady state,
 184 but had no qualitative effect on results or conclusions of the present study. Note also that in our
 185 present model, homeostatic synaptic plasticity scaled all PY-PY synaptic conductances by the
 186 same amount, and all PY-IN conductances were scaled by the same amount as well (though
 187 different from that of PY-PY case). Because of this similarity across all synapses of the same
 188 type, we could quantify the extent of homeostatic synaptic plasticity simply by computing the
 189 percentage of change in synaptic conductance relative to its value in the baseline model. Thus,

$$190 \quad \text{taking PY-PY synapse as an example, } HSP \equiv 100 \cdot \frac{G_{PP}(t=T) - G_{PP}(t=0)}{G_{PP}(t=0)}, \text{ where the time } T \text{ is}$$

191 taken to be sufficiently long after the trauma event (in the new post-traumatic steady state).

192

193 *Analysis of network structure*

194 We applied several widely used measures to characterize organization of the intact subnetwork.
 195 The interconnectedness of the intact subnetwork was quantified by computing the network
 196 averaged in-degree $\langle k_i \rangle$, the mean number of incoming connections received by a typical intact
 197 neuron from other intact neurons. To quantify the topological correlations in the subnetwork of

198 intact neurons, we computed its clustering coefficient. The clustering coefficient of i -th intact
199 neuron was defined as

$$200 \quad c_i = \frac{\sum_{j=1, m=1}^{N_K} e_{ij} e_{im} e_{jm}}{N_K (N_K - 1)} \quad (12)$$

201 where N_K is the number of intact neurons that send synaptic connections to the i -th intact
202 neuron, $e_{ij} = 1$ if j -th intact neuron projects a synapse to i -th intact neuron (and $e_{ij} = 0$ if there
203 is no such synaptic connection) and the double sum runs over all pairs of intact neurons that
204 send synaptic connections to i -th intact neuron. The clustering coefficient measures the
205 abundance of "connectivity triangles" and thus can be used to estimate the number of
206 elementary recurrent circuits in the subnetwork of presynaptic intact neurons that send synapses
207 to a given intact neuron. A network averaged clustering coefficient of intact subnetwork was
208 obtained by averaging c_i over all intact neurons.

209

210 In a set of simulations, we replaced the intact subnetworks with their equivalent random graphs.
211 These graphs were composed of the same set of intact neurons N_i , had the same mean in-
212 degree $\langle k_i \rangle$ (same averaged number of synapses from other intact neurons to a given neuron)
213 but uniform probability $p_{ij} = (N_i - 1) / \langle k_i \rangle$ to establish a pair-wise connection between intact
214 neurons, and were characterized by a much lower clustering coefficient as compared to the
215 intact subnetworks of the baseline model from which they were derived (see Figure 1 for
216 schematic diagram; see also Figure 4A for quantification of clustering coefficient reduction).

217

218 As we show in Results, the mean number of incoming connections in intact subnetworks
219 increased as the density of intact neurons increased. Thus, either one of these parameters
220 (incoming connectivity or spatial density of intact neurons) could in principle affect the rate of

221 paroxysmal discharges. To clearly determine the relative role of connectivity vs. spatial density,
222 in another set of simulations we replaced the intact subnetworks with a network that had preset
223 connectivity (the same mean number of incoming connections per intact neuron was used for
224 subnetworks with different spatial distribution of their neurons). Specifically, for each density
225 scenario we determined the intact neurons (same number of intact neurons was used regardless
226 of their spatial density), and then imposed synaptic connections between them (same mean
227 number of synapses to a given intact neuron from other intact neurons was used, regardless of
228 their spatial density), in addition to synaptic connections those intact neurons formed with
229 deafferented neurons (Figure 1). This allowed us to avoid mixing the effects of spatial
230 distribution of intact neurons with the changes in their interconnectedness in the intact
231 subnetwork.

232

233

234 **Results**

235

236 **Rate of post-traumatic IEDs depends on the spatial distribution of intact neurons**

237

238 To study effects of synaptic deafferentation on the network dynamics we designed large-scale
239 network model of the cortical excitatory neurons and inhibitory interneurons (see Methods) that
240 displayed random asynchronous activity in the physiological frequency range (Figure 2A).
241 Immediately following the deafferentation, the averaged firing rate of pyramidal neurons
242 dropped to the very low levels (< 1 Hz) (Figure 2B). Synaptic interactions significantly
243 contributed to neuronal dynamics in our model: Thus, after deafferentation the firing rate of
244 intact neurons was also reduced. The extent of the drop in the firing rate of intact neurons
245 depended on the parameters for deafferentation and on the spatial density of intact neurons (e.g.
246 for scenario considered in Figure 2C the initial drop in averaged firing rate of intact neurons
247 was from 5 Hz to ~ 0.4 Hz, but for scenario considered in Figure 2D the initial drop was from 5
248 Hz to ~ 3 Hz). Evidence from experimental studies and clinical data suggests that post-traumatic
249 networks undergo significant remodeling of anatomical and functional connectivity that aims to
250 compensate for the trauma-induced reduction of excitability and activity (Dyhrfeld-Johnsen et
251 al. 2007; Butz et al. 2009; Jin et al. 2006; Avramescu and Timofeev 2008). In particular,
252 trauma-induced acute reduction of activity may modify synaptic strengths by activating
253 homeostatic synaptic plasticity (HSP) (Avramescu and Timofeev 2008), which up-regulates
254 depolarizing influences (e.g., excitatory intrinsic and synaptic conductances) and down-
255 regulates hyperpolarizing ones (e.g., inhibitory conductances) (Turrigiano et al. 1998). This
256 regulatory process depends on the ongoing network activity and operates on a faster time-scale
257 than do the mechanisms of structural network reorganization (e.g., post-traumatic sprouting, see

258 (Dyhrfeld-Johnsen et al. 2007; Morgan and Soltesz 2008)). We implemented HSP in our model
259 of post-traumatic network reorganization.

260

261 In our model, homeostatic regulation adjusted the strengths of synaptic conductances to bring
262 the network-averaged firing rate to a preset target level of 5 Hz corresponding to a typical rate
263 of asynchronous firing in intact neocortex (Figure 2E). We previously demonstrated that HSP-
264 mediated up-regulation was able to recover normal asynchronous spiking activity for low to
265 moderate levels of deafferentation only (Houweling et al. 2005; Frohlich et al. 2008). A result
266 of homeostatic regulation following severe deafferentation was the transformation of collective
267 activity from asynchronous (for “healthy” cortex, Figure 2A) to burst-like activity (Figure 2B-
268 D) that resembled the IEDs; each burst lasted ~200 ms and gradually recruited all model
269 neurons. Importantly, however, here we found that the effect of HSP on the mean firing rate
270 depended on the spatial distribution of intact neurons (see definition of “intact neuron density”
271 in Methods), with low density scenarios (intact neurons widely scattered in space; low ρ_I)
272 resulting in failure to achieve the preset rate for physiological levels of synaptic scaling
273 (maximal up-regulation limited at 100%, corresponding to the double of the initial synaptic
274 strength, as in (Turrigiano et al. 1998)). The rate at which bursts were generated depended on
275 the density, ρ_I , of intact sub-population (Figure 2B-D). The bursts emerged only after
276 homeostatic plasticity changed synaptic conductances to become sufficiently strong, suggesting
277 that this mode of collective activity depends on synaptic interactions. In lower density
278 scenarios, model neurons fired more spikes per burst compared to the higher density scenario
279 (compare middle panels in Figure 2B-D) thus compensating for the lower burst rate and helping
280 to bring the network average firing rate of PY neurons toward its target value. Taken together
281 with the apparent dependence of post-traumatic burst rate on spatial distribution of intact
282 neurons, this suggests that the network organization of a small set of coupled intact neurons

283 may significantly affect post-traumatic activity in a whole network; this important issue was the
284 focus of the current study.

285

286 **Topological determinants of intact subnetwork correlate with the rate of post-traumatic** 287 **IEDs**

288

289 We now quantify the effects of the spatial distribution of intact neurons on reorganization of
290 collective activity in post-traumatic network. The spatial density of intact neurons was varied by
291 uniformly distributing them in square blocks of preset dimensions. We found that the rate at
292 which IEDs were generated significantly changed with the density of intact neurons ρ_I (Figure
293 3A). The asymptotic (after a sufficiently long time) level of homeostatic synaptic scaling
294 increased for the network with a low density of intact neurons until it saturated at 100% (Figure
295 3B). For a given spatial density, the rate of IEDs depended nonlinearly on deafferentation - the
296 amount of reduction in the rate of extra-layer afferent stimulation (see below, Figure 6A).
297 Earlier studies by other groups (Netoff et al. 2004; Dyhrfeld-Johnsen et al. 2007; Bogaard et al.
298 2009) suggested that changes of the network topology (e.g., averaged number of incoming
299 connections per neuron, clustering coefficient of a network, or minimal path length) can lead to
300 epileptic-like activity. To understand how the network organization of a small number of intact
301 neurons that survived the trauma determines the chances of generating collective interictal
302 dynamics in our model networks, we computed the clustering coefficient of the directional
303 graph that described subnetwork ω of intact neurons ($\omega \subset \Omega$, where Ω denotes the entire
304 network), for different spatial densities of intact neurons. A clustering coefficient of i -th neuron,
305 c_i , measures the abundance of "connectivity triangles" (elementary recurrent circuits) in the
306 subnetwork defined by that neurons' projections from other intact neurons (Methods); thus,
307 higher c_i is expected to lead to a more correlated, and possibly stronger, excitation of the i -th

308 neuron. As is seen from Figure 3C, in our networks the distribution of c_i was much broader
309 with high peak near zero when intact neurons were scattered in low density, as compared with
310 the high density scenario in which the intact neurons were clustered in space. The network-
311 averaged clustering coefficient of intact subnetwork was positively correlated with the rate of
312 IEDs that engulfed the entire traumatized network (Figure 3E), and was also positively
313 correlated with the spatial density of intact neurons (Figure 3D). Thus, we conclude, that
314 topological determinants of network structure positively correlate with the rate of paroxysmal
315 burst generation.

316

317 **Spatial density, but not topology, of intact subnetwork is causal in increasing the rate of**
318 **IEDs in traumatized network**

319

320 Is the rate of paroxysmal discharges in post-traumatic network determined solely by the
321 topological organization of intact subnetwork? Both the clustering coefficient and the mean
322 number of collateral synapses, $\langle k_i \rangle$, between intact neurons scaled up with the density of intact
323 neurons (Figures 3D,F). In general, these two characteristics of the network topology are
324 independent and the observed burst rate increase after deafferentation could be conflated with
325 either of them or with both. Alternatively, the burst rate increase can be primarily mediated by
326 increase of the spatial density of intact neurons. To answer this question, in simulations below,
327 we alternated the connectivity structure of the population of intact neurons that “survived”
328 deafferentation.

329

330 To determine the role of topological clustering in paroxysmal burst generation, we substituted,
331 immediately after deafferentation, the equivalent random graph for the subnetwork ω of all
332 intact neurons. This graph consisted of the same set of intact neurons with each neuron

333 receiving the same averaged number of synapses from other intact neurons but probability to
334 establish a pair-wise connection between intact neurons was uniform (see Methods). Such
335 randomization of intact subnetwork topology significantly reduced the average clustering
336 coefficient of the network (Figure 4A), while resulting in a small but significant decrease in the
337 incidence of post-traumatic paroxysmal bursts (Figure 4B). Thus, a higher clustering coefficient
338 correlated with an increased rate of paroxysmal discharge, but explained only a small part of it.

339

340 To assess the extent to which increased number of collateral synapses in the intact subnetwork
341 affects the rate of paroxysmal discharges, we substituted, immediately after deafferentation, the
342 network with fixed connectivity for the subnetwork ω of all intact neurons. Specifically, we
343 replaced connectivity between intact neurons by fixed connectivity with the same mean number
344 of synapses regardless of the spatial density of intact neurons (see Methods). Thus, in this fixed
345 connectivity network the structure and number of synapses between intact neurons was kept
346 constant regardless of their density (Figure 4C). Interestingly, in the networks with fixed
347 connectivity, the rate of IEDs still showed a very strong dependence on the spatial density of
348 intact neurons (Figure 4D). When density was low, synaptic drive to deafferented neurons from
349 intact ones was insufficient to initiate spikes required for global activity propagation regardless
350 of the connectivity pattern between intact neurons. Thus, increased collateral connectivity of
351 intact subnetwork correlated with the increased rate of paroxysmal discharge, but also explained
352 only a small part of it.

353

354 Network averaged minimal path length defines the averaged number of connected neurons that
355 separate any two neurons in the network. Minimal path length is relatively low in networks with
356 random structure of synaptic connectivity. It has been suggested that the low path length could
357 facilitate fast signal propagation in networks (Dorogovtsev and Mendes 2003); thus, it could

358 also affect the rate at which paroxysmal events are generated (Netoff et al. 2004). However, our
359 results suggest that in our model, path length is not causally related to the rate of burst
360 generation. Indeed, in a network with fixed connectivity (Figure 4C) path length was also fixed
361 (path length was 2 for the case $\langle k_i \rangle = 12$, and was 1.75 for the case $\langle k_i \rangle = 24$), but that did not
362 in itself eliminate the increase in burst rate with increasing spatial density of intact neurons
363 (Figure 4D). Furthermore, the rate of paroxysmal bursts was nearly the same between two
364 networks with different path length.

365

366 Collectively, these results suggest that the topological parameters of a network of intact neurons
367 that "survived" deafferentation only weakly affected the form of post-traumatic activity;
368 nonetheless, the spatial density of trauma-surviving neurons *per se* had a dominant role.

369

370 **Patterns of electrical activity are modulated by properties of synaptic transmission at PY-**
371 **PY synapses**

372

373 Since burst initiation and propagation in our networks critically relied on synaptic interactions,
374 we wanted to further elaborate the extent to which properties of synaptic transmission (in
375 particular at PY-PY synapses) could shape collective activity in post-traumatic networks. We
376 focused on the effects of NMDA conductance and short-term synaptic depression at PY-PY
377 synapses.

378

379 In principle, burst initiation could be affected by the NMDA conductance at PY-PY synapses.
380 Initiation of intense bursting requires effective summation of activity from several presynaptic
381 neurons. Given the relatively slow time scale of NMDA current decay, it could affect the
382 excitability of post-synaptic neuron, affect temporal summation of excitatory input from

383 collateral synapses, and thus affect the propensity for burst generation. We tested the role of
384 slow NMDA currents by removing NMDA conductance from PY-PY synapses. Removal of
385 NMDA conductance from PY-PY synapses had dramatic effects on the properties of collective
386 electrical activity in post-traumatic networks (Figure 5). For sufficiently high density of intact
387 neurons, bursts were generated at high rate (Figure 5A) and propagated through the network as
388 sharp waves during which each model neuron fired at most 1 action potential (Figure 5C,
389 middle panel, compare to the top panel for baseline model network). Homeostatic synaptic
390 scaling in these networks without NMDA conductance attained highest allowed values
391 (maximal up-regulation of 100 percent, Figure 5B), yet the network averaged firing rate of PY
392 neurons failed to reach the target value of 5 Hz. Notably, below a critical spatial density the
393 characteristics of electrical activity (burst rate, HSP scaling factor) were the same for baseline
394 model networks and for networks without NMDA conductance. Thus, we conclude that NMDA
395 conductance at PY-PY synapses can modulate the pattern of collective electrical activity (by
396 increasing the number of spikes fired by a PY model neuron per burst, thus increasing the mean
397 neuronal firing rate and decreasing the rate of paroxysmal discharges), but its effects again
398 depended on the spatial density of intact neurons. Without NMDA conductance, the target
399 values of the network firing rate could be only achieved as a result of extreme up-regulation of
400 the fast excitatory synapses that led to the very high level of synchrony of firing.

401

402 Synaptic transmission could also be affected by the presence of short-term synaptic depression,
403 which was incorporated at PY-PY synapses in our model network. The strength of synaptic
404 depression in our model was characterized by “resource usage” parameter U that quantified
405 how much “synaptic resource” was used by a synapse per each synaptic spike (lower values of
406 U mean milder depression). Reducing U to 50% of its baseline value led to a reduction in
407 burst rate (Figure 5A, green diamonds vs. black squares). At the same time, bursts became

408 wider, with each model neuron firing intensely during the bursting event (Figure 5C, bottom
409 panel). The amount of HSP at model synapses and the mean firing rate of PY neurons were also
410 affected (Figures 5B,D). When synaptic depression was completely removed from PY-PY
411 synapses, bursts were generated at a very low rate (0.035 Hz, data not shown), but each bursting
412 event lasted about 5 seconds, with neurons firing intensely during the entire burst, similar to
413 seizure-like activity.

414

415 Thus, properties of synaptic transmission at PY-PY synapses could modulate the emerging
416 pattern of collective activity in post-traumatized networks. With only weak depression of
417 synaptic coupling between pyramidal neurons, collective activity resembled seizures (periods of
418 intense activity each lasting several seconds) occurring at a low rate. Stronger depression led to
419 earlier burst termination and promoted generation of paroxysmal-like network bursts of short
420 duration at higher rate. In all cases, the rate at which these bursts were generated critically
421 depended on the spatial density of intact neurons.

422

423 **Functional severity of cortical trauma affects initiation and propagation of paroxysmal** 424 **bursts**

425

426 The spatial density of intact neurons affects the rate of IEDs through strong excitation of nearby
427 deafferented neurons, which occurred because of the larger number of intact neurons, firing at a
428 relatively high rate, projecting to a given deafferented neuron and promoted burst propagation
429 through the network in spite of low excitability of traumatized neurons. A single intact neuron is
430 not likely to excite its postsynaptic deafferented target to a point of spike generation. However,
431 when several intact neurons are close enough in space, there is a possibility that they are
432 synaptically coupled, as well as share one or more postsynaptic targets. Thus, there is an

433 increased chance for activity to be propagated through the intact subnetwork, and intact neurons
434 can provide stronger input to nearby deafferented neurons, increasing the chance for the latter to
435 fire action potentials. Upregulation of synaptic conductances by homeostatic synaptic plasticity
436 increases synaptic coupling and so would further increase the excitation of deafferented neurons
437 by their intact peers. We reasoned that neuronal excitability (partially controlled in our networks
438 by parameter r_D : the remaining rate of afferent stimulation of traumatized neurons after
439 deafferentation) could also affect the rate of post-traumatic paroxysmal bursts. As Figure 6A
440 shows, the burst rate peaked for a certain, density-invariant, value of r_D , with low rates of
441 activity both for strong (low r_D) and mild (high r_D) trauma scenarios. The amount of HSP
442 needed to reach these levels of activity was a monotonic increasing function of trauma severity
443 (Figure 6C).

444

445 One interesting observation from Figure 6A is that the rate of paroxysmal discharges depended
446 on the spatial density of intact neurons (characterized by ρ_I) only in the severe trauma regime
447 (small r_D) and was largely independent of the spatial density for milder trauma (high r_D). To
448 understand why this difference between severe and mild trauma regimes arose, we computed
449 the standard deviation of firing rate of all PY neurons in the network (Figure 6B). In mild
450 trauma regime, standard deviation of PY neurons firing rates was largely the same for all
451 density scenarios, and attained smaller values for higher r_D (milder trauma). This suggests that
452 in mild trauma regime, deafferented neurons become more like their intact peers. The milder the
453 trauma, the less is the drop in afferent stimulation, and deafferented neurons are more excitable
454 immediately after deafferentation. In addition, for milder trauma HSP is able to compensate for
455 a reduction in firing rate incurred by a relatively small decrease in afferent excitation. Thus, in
456 this scenario the excitability level of deafferented neurons is close to that of their intact peers.
457 Consequently the exact spatial configuration of intact neurons (a critical factor which

458 determines the ability of an intact subnetwork to engage the deafferented neurons paroxysmal
459 burst) becomes less important, thus blurring the role of spatial density. By the same token, the
460 differences between intact and deafferented neurons becomes more pronounced in severe
461 trauma regimes (low r_D), thus underscoring the role that spatial configuration of intact
462 subnetwork has in burst generation (Figure 6A, severe trauma regime).

463

464 Another interesting feature seen in Figure 6A is that, for medium and low spatial density of
465 intact neurons (low ρ_I) the rate of paroxysmal discharges exhibited a peak when plotted vs. the
466 functional severity of trauma, r_D . We explain this finding using the following heuristic
467 argument: First, note that the HSP is strongest for most severe trauma and then monotonically
468 reduces for milder trauma (Figure 5D); Second, note that the excitability of an isolated model
469 neuron that is driven only by afferent external input increased for milder trauma (Figure 6C) vs.
470 more severe trauma. This offers the following explanation for the non-monotonic dependence of
471 the burst rate on the severity of trauma: Quite generally, the rate of IEDs depends on two factors
472 - neuronal excitability and the strength of collateral synaptic connections. Excitability of
473 traumatized neurons is low in severe trauma cases (low r_D), making it unlikely that a network
474 can initiate and propagate global IEDs, despite the very strong synaptic conductance that is
475 scaled up by HSP to its maximum value at 100%. Those events require correlated activity of
476 remaining intact neurons and are therefore rarely generated in the network of randomly spiking
477 cells. On the other hand, in a mild trauma scenario (high r_D), neurons are relatively excitable
478 and noisy, but collateral connections even after HSP up-regulation are not strong enough to
479 ensure reliable propagation of correlated burst. Thus, in this limit the network favors the
480 asynchronous mode over the IEDs. For traumatic events of a moderate severity, IEDs can be
481 generated at the highest rate that is limited by the balance of intrinsic (remaining rate of afferent
482 stimulation) and synaptic (HSP) excitability (Figure 6E).

483

484

485 **Discussion**

486

487 Alterations in network connectivity can significantly promote epileptogenesis through
488 establishment of long-range connections which lead to the formation of "small-world" networks
489 (Netoff et al. 2004; Dyhrfeld-Johnsen et al. 2007). Here, we studied the emergence of IEDs in
490 the deafferentation model of post-traumatic epileptogenesis. Our results suggest that structural
491 change in connectivity might be a sufficient, but not a necessary condition for the generation of
492 IEDs. In our model, bursting depended on the change in the functional connectivity (the extent
493 to which one neuron can affect another) of intact subnetwork, as well as on the ability of the
494 traumatized network to convey the burst that was generated by the intact neurons. Thus, we
495 showed that the geometrical organization of a small number of trauma-surviving neurons can be
496 a decisive factor in determining the properties of post-traumatic IEDs.

497

498 The mechanism by which a small number of intact neurons affected burst generation in our
499 model was based on their geometrical organization. Because of the local synaptic footprint,
500 intact neurons had to be proximal enough in space in order to be able to form recurrent
501 connections between them and also to create a situation in which nearby deafferented neurons
502 would have sufficiently large number of synaptic contacts from their intact peers. Proximity of
503 intact neurons elevated their firing rates by means of their synaptic interaction, which
504 consequently elevated the excitation of deafferented neurons. Homeostatic synaptic plasticity
505 further upregulated synaptic coupling strength and thus also contributed to the increased firing
506 rate of intact neurons and to the increased excitation of nearby deafferented neurons. When
507 sufficiently excited by their intact peers, deafferented neurons generated action potentials that

508 further propagated through the network of deafferented neurons in form of paroxysmal burst.
509 Synaptic depression and time course of synaptic conductance (slow NMDA) affected the time-
510 dependent strength of synaptic coupling and thus modulated the rate of paroxysmal burst
511 generation.

512

513 In the model presented in this study we assumed a population of intact neurons embedded in a
514 “sea” of traumatized neurons. Thus, we implicitly assumed that even in what might appear to be
515 a completely deafferented piece of cortical tissue, there might be some small number of neurons
516 that preserve their intact afferent input after deafferentation. In reality, trauma is more likely to
517 create a traumatized region surrounded by the intact network; however, in this situation it is
518 difficult to correctly define the spatial density of intact neurons. Experimental data (Topolnik et
519 al. 2003) and our preliminary modeling results suggest that paroxysmal bursts were generated
520 by intact neurons at the boundary between traumatized and intact regions. Nevertheless, we
521 chose in this study to focus on the effects of spatial density and investigate the scenario in
522 which a small set of intact neurons is embedded in a large traumatized network.

523

524 Netoff et al. (2004) showed, in a computational model of hippocampal network, that bursting
525 (but not seizing) is facilitated in networks with low clustering coefficient and short path length.
526 Analysis of in-vitro glutamate injury models of hippocampal neuronal networks led to the same
527 conclusion – an increase in burst rate was accompanied by a strong reduction in network
528 clustering coefficient (Srinivas et al. 2007). Our own results suggest that while clustering
529 coefficient of intact subnetwork positively correlates with the rate of interictal events, in itself it
530 is not a causal factor leading to the IED generation. Significant change of the clustering
531 coefficient in the model led to only slight change of the burst rate. However, those earlier
532 studies focused on epileptogenesis in networks of cells with homogeneous excitability

533 properties. By contrast, in our model the trauma created two populations of neurons
534 (deafferented and intact) with different excitability properties. Subsequent action of HSP only
535 increased this difference. Burst generation depended on the ability of the intact population to
536 “ignite” the deafferented population of neurons. This differs from the conclusions of earlier
537 studies (Netoff et al. 2004; Srinivas et al. 2007) in which bursting depended on the ability to
538 quickly propagate spikes in a network of neurons with same excitability. Indeed, neither one of
539 the topological parameters of our model (clustering coefficient and minimal path length
540 between model neurons) had a causal influence on the rate of paroxysmal discharges; however,
541 the rate of bursts was critically affected by the spatial density of intact neurons. Thus, in the
542 deafferentation model of post-traumatic epilepsy, structural changes in connectivity may be not
543 a primary factor in burst generation.

544

545 Earlier computational models stressed the importance of network interconnectedness (mean
546 number of synapses received by a neuron) in setting the rate of interictal bursting activity,
547 suggesting that more interconnected networks can generate bursts of collective activity at higher
548 rate (Figure 4C,F in (Netoff et al. 2004)). Our own results suggest that in the post-traumatic
549 epilepsy scenario, mean number of connections between intact neurons may not play a central
550 role – the rate of IEDs in model networks with fixed connectivity of intact subnetwork was
551 virtually indistinguishable from that of the baseline model (Figure 4C,D). At first, this may
552 appear to contradict the conclusions of an earlier study (Netoff et al. 2004). However, in
553 contrast to the IEDs induced by stronger recurrent connectivity (Netoff et al. 2004), the trauma
554 in our model of IEDs significantly reduced the network excitability by decreasing the afferent
555 excitation (captured by the parameter r_D in our model) thus making the post-traumatic network
556 harder to excite. We found that increasing mean number of connections between intact neurons
557 only increased the burst rate if it was accompanied by increasing mean number of projections

558 from intact neurons to deafferented cells. The last occurred when spatial density of intact
559 neurons was increased.

560

561 Homeostatic synaptic plasticity in post-traumatic cortical networks might be mediated by
562 diffusible tumor necrosis factor (TNF) alpha (Stellwagen and Malenka, 2006). This molecule is
563 believed to be released from astrocytes in response to neural trauma (Lau and Yu, 2001), and it
564 was shown that TNF alpha plays a critical role in synaptic scaling (Stellwagen and Malenka,
565 2006; Steinmetz and Turrigiano, 2010). Initially after traumatic event, astrocytic response
566 might create “patches” of high TNF alpha concentration co-localized with those parts of the
567 network that are more severely affected by the trauma. In such early post-traumatic scenario of
568 spatially heterogeneous trauma, the model of HSP will need to be critically revised to reflect the
569 dependence of HSP on local levels of synaptic inactivity. In contrast, our present model
570 assumes that HSP is evaluated based on the global, network-wide, level of inactivity, an
571 assumption which reflects the situation when the levels of TNF alpha have equilibrated by
572 diffusion (Edelstein-Keshet and Spiros 2002). This is likely to occur during the late stage of
573 post-traumatic reorganization, after the network has reached its new steady-state. Thus, our
574 present model might implicitly reflect the situation in the post-traumatic steady state. Our
575 preliminary results (to be published elsewhere) indicate that during the early post-traumatic
576 phase, the spatially localized action of the HSP might render the cortical network with strong
577 sensitivity toward local perturbations of electrical activity, thus potentially resulting in a high
578 rate of paroxysmal bursts. However, experimentally no (or very little) epileptic-like activity has
579 been observed immediately following the trauma. This suggests that the network might employ
580 additional, neuro-protective, mechanisms that would reduce the rate of paroxysmal discharge in
581 spite of high sensitivity to perturbations. These mechanisms and their actions are being
582 investigated in ongoing work.

583

584 The HSP that followed the deafferentation in our model increased connectivity strength which
585 in turn increased the firing rate of intact neurons. However, this increased firing rate was not
586 always communicated to the rest of the network – only in special space configurations
587 (relatively high density of intact neurons) could intact neurons collectively nucleate sufficiently
588 strong activity that initiated spiking in deafferented neurons and took the form of IEDs
589 propagating through the cortical network. Thus, the excitability and the spatial distribution of a
590 small number of neurons that preserved their inputs after trauma, overshadows the role of
591 network topology and connectivity in the generation of post-traumatic IEDs. Several studies
592 have indicated that topological correlation in connectivity can enhance burst generation
593 (Bogaard et al. 2009; Dyhrfeld-Johnsen et al. 2007); however, this can be heavily affected by
594 the dynamics of neuronal excitability. Thus, more detailed studies, aiming to investigate the
595 interplay of trauma pattern, synaptic connectivity and intrinsic neuronal excitability, are
596 required to understand the emergence of pathological rhythms in traumatized brain.

597

598

599 **Acknowledgements**

600

601 This research was supported by the NIH grant R01 NS059740 and the Howard Hughes Medical
602 Institute.

603

604 **References**

605

606 Avramescu S, Timofeev I. Synaptic strength modulation after cortical trauma: a role in
607 epileptogenesis. *J Neurosci* 28:6760-6772, 2008.

608

609 Bogaard A, Parent J, Zochowski M, Booth V. Interaction of cellular and network mechanisms
610 in spatiotemporal pattern formation in neuronal networks. *J Neurosci* 29:1677-1687, 2009.

611

612 Butz M, van Ooyen A, Worgotter F. A model for cortical rewiring following deafferentation
613 and focal stroke. *Frontiers Comput Neurosci* 3:10, 2009.

614

615 de Curtis M, Avanzini G. Interictal spikes in focal epileptogenesis. *Prog Neurobiol* 63:541-567,
616 2001.

617

618 Dorogovtsev SN, Mendes JFF. Evolution of networks: from biological nets to the Internet and
619 WWW. Oxford Univ Press USA, 2003.

620

621 Dyhrfeld-Johnsen J, Santhakumar V, Morgan RJ, Huerta R, Tsimring L, Soltesz I. Topological
622 determinants of epileptogenesis in large-scale structural and functional models of the dentate
623 gyrus derived from experimental data. *J Neurophysiol* 97:1566-1587, 2007

624

625 Dzhala VI, Staley KJ. Transition from interictal to ictal activity in limbic networks *in vitro*. *J*
626 *Neurosci* 23:7873-7880, 2003.

627

628 Edelstein-Keshet L, Spiros A. Exploring the formation of Alzheimer's disease senile plaques *in*
629 *silico*. *J Theor Biol* 216:301-326, 2002.

630

631 Frohlich F, Bazhenov M, Sejnowski TJ. Pathological effect of homeostatic synaptic scaling on
632 network dynamics in diseases of the cortex. *J Neurosci* 28:1709-1720, 2008.

633

634 Grafstein B, Sastry PB. Some preliminary electrophysiological studies on chronic neuronally
635 isolated cerebral cortex. *Electroencephalogr Clin Neurophysiol Suppl* 9:723-725, 1957.

636

637 Houweling AR, Bazhenov M, Timofeev I, Steriade M, Sejnowski TJ. Homeostatic synaptic
638 plasticity can explain post-traumatic epileptogenesis in chronically isolated neocortex. *Cereb*
639 *Cortex* 15:834-845, 2005.

640

641 Jin X, Prince DA, Huguenard JR. Enhanced excitatory synaptic connectivity in layer V
642 pyramidal neurons of chronically injured epileptogenic neocortex in rats. *J Neurosci* 26:4891-
643 4900, 2006.

644

645 Keller CJ, Truccolo W, Gale JT, Eskandar E, Thesen T, Carlson C, Devinsky O, Kuzniecky R,
646 Doyle WK, Madsen JR, Schomer DL, Mehta AD, Brown EN, Hochberg LR, Ulbert I, Halgren
647 E, Cash SS. Heterogeneous neuronal firing patterns during interictal epileptiform discharges in
648 the human cortex. *Brain* 133:1668-1681, 2010.

649

650 Lau LT, Yu ACH (2001) Astrocytes produce and release interleukin-1, interleukin-6, tumor
651 necrosis factor alpha and interferon-gamma following traumatic and metabolic injury. *J*
652 *Neurotrauma* 18: 351-359, 2001.

653

654 Morgan RJ, Soltesz I. Nonrandom connectivity of the epileptic dentate gyrus predicts a major
655 role for neuronal hubs in seizures. *Proc Natl Acad Sci USA* 105:6179-6184, 2008

656

657 Netoff TI, Clewley R, Arno S, Keck T, White JA. Epilepsy in small-world networks. *J Neurosci*
658 24:8075-8083, 2004.

659

660 Pitkanen A, Schwartzkroin PA, Moshe SL. Models of seizure and epilepsy (editors). Elsevier
661 Science, 2006.

662

663 Prescott SA, Ratte S, De Koninck Y, Sejnowski TJ. Nonlinear interaction between shunting and
664 adaptation controls a switch between integration and coincidence detection in pyramidal
665 neurons. *J Neurosci* 26:9084-9097, 2006.

666

667 Prince DA, Tseng GF. Epileptogenesis in chronically injured cortex: in vitro studies. *J*
668 *Neurophysiol* 69:1276-1291, 1993.

669

670 Srinivas KV, Jain R, Saurav S, Sikdar SK. Small-world network topology of hippocampal
671 neuronal network is lost, in an in vitro glutamate injury model of epilepsy. *Eu J Neurosci*
672 25:3276-3286, 2007

673

674 Steinmetz CC, Turrigiano GG. Tumor necrosis factor- α signaling maintains the ability of
675 cortical synapses to express synaptic scaling. *J Neurosci* 30: 14685-14690, 2010.

676

677 Stellwagen D, Malenka RC. Synaptic scaling mediated by glial TNF- α . *Nature* 440: 1054-1059,
678 2006.

679

680 Timofeev I, Bazhenov M, Avramescu S, Nita DA. Posttraumatic epilepsy: the roles of synaptic
681 plasticity. *Neuroscientist* 16:19-27, 2010.

682

683 Topolnik L, Steriade M, Timofeev I. Partial cortical deafferentation promotes development of
684 paroxysmal activity. *Cereb Cortex* 13:883-93, 2003.

685

686 Turrigiano GG, Leslie KR, Desai NS, Rutherford LC, Nelson SB. Activity-dependent scaling of
687 quantal amplitude in neocortical neurons. *Nature* 391:892-896, 1998.

688

689 Wendling F, Hernandez A, Bellanger JJ, Chauvel P, Bartolomei F. Interictal to ictal transition in
690 human temporal lobe epilepsy: insights from a computational model of intracerebral EEG. *J*
691 *Clin Neurophysiol* 22:343-356, 2005.

692

693

694 **Figure Legends**

695

696 **Figure 1**

697 Schematic diagram of manipulations to network connectivity schemes.

698 *Left:* The baseline subnetwork of intact neurons. Because synaptic footprint is local, distant
699 intact neurons are not connected.

700 *Center:* The subnetwork with randomized connectivity. Number of intact connections per intact
701 neuron is the same as in the baseline model, locations of intact neurons are the same, but the
702 correlation structure of connectivity is destroyed by allowing distant intact neurons to be
703 connected.

704 *Right:* The subnetwork with fixed connectivity. Number of intact connections per intact neuron
705 is the same as in the baseline model, and the correlation structure of connectivity is the same as
706 well. Spatial proximity between intact neurons is destroyed by randomly redistributing them
707 through the network.

708

709

710 **Figure 2**

711 Trauma induced transformation of network electrical activity.

712 A "Healthy" cortical network exhibited asynchronous activity, with PY neurons firing at ~5 Hz
713 and IN neurons firing at ~10 Hz.

714 **B,C,D** Examples of post-traumatic steady state collective activity (left) for different spatial
715 patterns of trauma parameterized with different spatial densities ρ_I of intact neurons (right). In
716 the left plots, Y axis indexes the 250 sampled neurons. In center panels, we show temporal
717 profiles of representative paroxysmal bursts for each scenario. In right plots, black dots denote
718 the intact neurons that survived the trauma. The white space within the boxes represents the
719 deafferented neurons that lost their afferent excitation following the trauma. Because we
720 considered cases of severe deafferentation (only up to 5 percent of network neurons survive the
721 trauma) the density (definition given in Methods) of intact neurons is close to 1 for all cases
722 considered.

723 **E** Following deafferentation, the network-averaged PY firing rate dropped dramatically, but
724 then slowly recovered due to the action of HSP. Temporal dynamics (fluctuations) of the firing
725 rate depended on the spatial pattern of deafferentation. Each dot represents network-averaged
726 firing rate of model pyramidal neurons in the window of 4 seconds. Different colors correspond
727 to the different spatial densities ρ_I of intact neurons: green line - $\rho_I = 0.02$, red line -
728 $\rho_I = 0.06$, black line - $\rho_I = 1$. In all panels (**B-E**), the number of intact neurons was the same
729 ($N_I = 100$).

730

731

732

733 **Figure 3**

734 Post-traumatic interictal activity depends on spatial organization of trauma-surviving neurons.

735 **A** Burst rate vs. spatial density of intact neurons. Number of intact neurons: $N_I = 100$

736 (squares); $N_I = 400$ (circles).

737 **B** Amount of HSP at model synapses. Symbols are the same as in **(A)**.

738 **C** Distributions of local clustering coefficient in intact subnetwork.

739 **D** Averaged clustering coefficient of intact subnetwork plotted vs. the spatial density of intact

740 neurons.

741 **E** Burst rate plotted vs. the network averaged clustering coefficient.

742 **F** Mean number of collateral intact synapses, vs. density of intact neurons. Data points are mean

743 \pm S.E.M. (N=4).

744

745

746

747 **Figure 4**

748 Network topology weakly affects paroxysmal activity.

749 **A** Network-averaged clustering coefficient for baseline intact network (squares) and equivalent
750 randomized network (circles) vs. the density of intact neurons.

751 **B** Burst rate plotted vs. the density of intact neurons, for scenarios considered in (**A**).

752 **C** Mean number of intact synapses per intact neuron in baseline intact network (squares) and
753 intact network with fixed connectivity (green diamonds, $\langle k_I \rangle = 12$; red circles, $\langle k_I \rangle = 24$) vs.
754 the spatial density of intact neurons.

755 **D** Burst rate plotted vs. the spatial density of intact neurons, for scenarios considered in (**C**). For
756 all cases, $N_I = 100$ and $r_D = 0.1$. Data points are mean \pm S.E.M. (N=4).

757

758

759

760 **Figure 5**

761 Properties of synaptic transmission modulate collective electrical activity in post-traumatic
762 network.

763 **A** Burst rate vs. the spatial density of intact neurons, for different scenarios of synaptic
764 transmission at PY-PY synapses: the baseline model with synaptic depression and NMDA
765 conductance at PY-PY synapses (black squares), the model with synaptic depression but
766 without NMDA conductance at PY-PY synapses (red circles), the model without synaptic
767 depression but with NMDA conductance at PY-PY synapses (green diamonds).

768 **B** Amount of HSP at model PY-PY synapses, for different scenarios shown in (A). Data keys
769 are the same ones as in (A).

770 **C** Representative sample raster plots of collective electrical activity for different scenarios
771 shown in (A): the baseline model (top panel), the model without NMDA conductance (middle
772 panel), the model without synaptic depression (bottom panel). For all plots, $\rho_I = 1$ (all the
773 neurons within selected area in the middle of the network are intact).

774 **D** Network averaged firing rate of PY model neurons for different scenarios shown in (A). Data
775 keys are the same ones as in (A).

776

777 **Figure 6**

778 Reduction in the rate of afferent excitation determines the propensity for burst generation.

779 **A** Burst rate plotted vs. the rate drop parameter, r_D , for different densities of trauma-surviving
780 neurons: $\rho_I = 1$ (black squares); $\rho_I = 0.06$ (red circles); $\rho_I = 0.02$ (green diamonds).

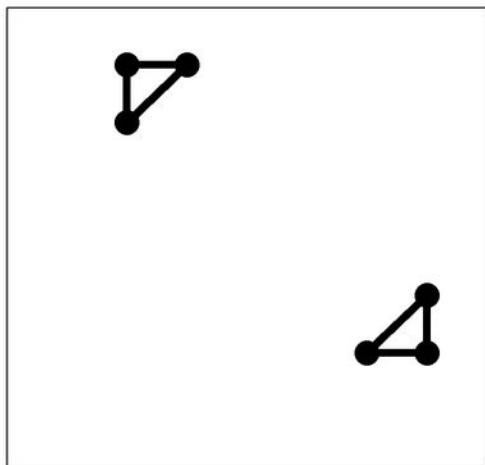
781 **B** Standard deviation (across all PY neurons) of firing rates of PY model neurons, plotted vs.
782 the rate drop parameter, r_D . Symbols are the same as in **(A)**.

783 **C** Firing rate of isolated neuron, plotted vs. r_D . Data points are averages over 100 neurons.

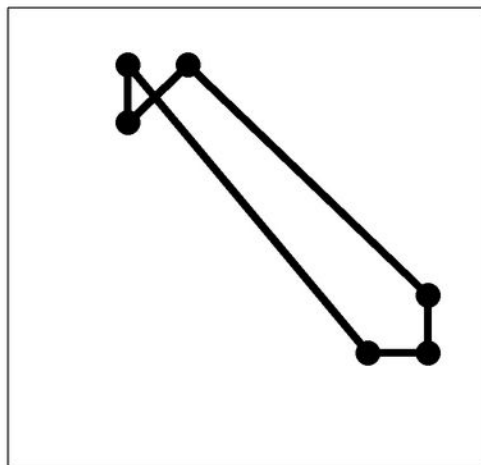
784 **D** Amount of HSP at model synapses. Symbols are the same as in **(A)**. In **(A, B, D)** data points
785 are mean \pm S.E.M. (N=4).

786 **E** Schematic presentation showing how the peak burst rate arises due to the competing action of
787 intra-cellular excitability (black line, strong for mild trauma) and homeostatic synaptic plasticity
788 (gray line, strong for strong trauma). Hypothetical burst rate is dashed red line (not to scale).

BASELINE MODEL



EQUIVALENT RANDOM GRAPH



FIXED CONNECTIVITY

